An unpredicted aggregation-critical region of the actin-polymerizing protein TRIOBP-1/Tara, determined by elucidation of its domain structure

Nicholas J. Bradshaw*[,1,2], Antony S. K. Yerabham*, Rita Marreiros*, Tao Zhang[‡,§], Luitgard Nagel-Steger[‡,§] and Carsten Korth*[,3]

From the *Department of Neuropathology and the [‡]Institute of Physical Biology, Heinrich Heine University, 40225 Düsseldorf, Germany and the [§]Institute of Complex Systems, Structural Biochemistry (ICS-6), Forschungszentrum Jülich, 52425 Jülich, Germany

Running title: *TRIOBP-1 domain structure and aggregation*

[1]Current address: Department of Biotechnology, University of Rijeka, 51000 Rijeka, Croatia

[2]To whom correspondence may be addressed: Odjel za biotehnologiju, Sveučilište u Rijeci, Radmile Matejčić 2, 51000 Rijeka, Croatia; E-mail: nicholas.bradshaw@hhu.de

[3]To whom correspondence may be addressed: Institut für Neuropathologie, Heinrich Heine Universität Düsseldorf, Moorenstraße 5, 40225 Düsseldorf, Germany; Telephone: +49 211 8116153; Fax: +49 211 8117804; E-mail: ckorth@hhu.de.

Keywords: Actin, Domain structure, Mental illness, Oligomerization, Protein aggregation, Protein stability, Schizophrenia, Subcellular localization, Tara, TRIOBP

ABSTRACT

Aggregation of specific proteins in the brains of patients with chronic mental illness as a result of disruptions in proteostasis is an emerging theme in the study of schizophrenia in particular. Proteins including DISC1 (Disrupted in Schizophrenia 1) and dysbindin-1B are found in insoluble accumulations within brain homogenates from such patients. We recently identified TRIOBP-1 (Trio-Binding Protein 1, also known as Tara) to be another such protein through an epitope discovery and proteomics approach, comparing *post mortem* brain material from schizophrenia patients and control individuals. We hypothesized that this was likely to occur as a result of a specific subcellular process, and that it therefore should be possible to identify a region of the TRIOBP-1 protein which is essential for its aggregation to occur.

Here, we probe the domain organization of TRIOBP-1, finding it to possess two distinct coiled coil domains: the central and C-terminal domains. The central domain inhibits the de-polymerization of F-actin and is also responsible for oligomerization of TRIOBP-1 and, along with an N-terminal Pleckstrin homology domain, affects neurite outgrowth.

In neuroblastoma cells, it was found that the aggregation propensity of TRIOBP-1 arises from its central domain, with a short "linker" region, narrowed to within amino acids 324-348, between its first two coiled-coils being essential for the formation of TRIOBP-1 aggregates. TRIOBP-1 aggregation therefore appears to occur through one or more specific cellular mechanisms, which therefore have the potential to be of physiological relevance for the biological process underlying the development of chronic mental illness.

The *TRIOBP* (*Trio-Binding Protein*) gene encodes for two distinct proteins (1,2), both of which are implicated in the modulation of actin, although the exact mechanisms by which they do this remain unclear (3,4). Of these TRIOBP-4, encoded by the 5' end of the gene, is a largely disordered protein (5), expressed principally in the inner ear and implicated in

deafness (1,2,4), while the 3'-encoded TRIOBP-1 protein is predicted to be folded (3) and is more ubiquitously expressed (1,2). The TRIOBP-1 protein is also known as Tara (Trio-Associated Repeat on Actin). Longer proteins containing the reading frames of both TRIOBP-1 and TRIOBP-4 also exist (1,2) but are less well characterized.

Recently, we performed an antibody-based screen for proteins which specifically form insoluble aggregates in the brains of patients with schizophrenia (6). This was based on the theory that disrupted protein homeostasis in post-mitotic neurons is likely to characterize subtypes of chronic mental illness (7). In this manner, an antibody against TRIOBP-1 was found to show specificity for the pooled purified insoluble protein fractions of *post mortem* brain samples from schizophrenia patients, compared to an equivalent preparation prepared from brain samples of control individuals (8). Further analysis determined the TRIOBP-1 protein, but not TRIOBP-4, to readily form insoluble aggregates when expressed in cell culture systems or primary neurons, implicating aggregation of TRIOBP-1 in mental health (8).

The specific roles of TRIOBP-1 in the brain are not well studied, however more generally it is known to be a critical promoter of actin polymerization, binding directly to polymerized fibres of F-actin (3,9). It is also involved in chromosome segregation during mitosis (10), as well as in cell migration. The latter occurs through its interaction with Nuclear Distribution Element-Like 1 (NDEL1) (11), a protein of significant importance in neurodevelopment which has been implicated in schizophrenia (12). Small, but statistically significant, increases in *TRIOBP* transcript expression have also been detected in *post-mortem* brain tissue of schizophrenia patients from two independent samples (13).

The misassembly of TRIOBP-1 protein into insoluble aggregates in mental illness could arise either because the protein is naturally "sticky", with a tendency to self-interact in a non-specific manner, or as the result of a specific physiological mechanism. Such mechanisms could include, for example, the addition or removal of a protein-binding partner, a post-translational modification, interaction with a small molecule or an error during protein folding. We hypothesized that, were a specific mechanism involved, it should be possible to isolate individual regions of the protein which were involved in this process (either small motifs or entire folded domains) and which are therefore required for aggregation of TRIOBP-1.

In this manuscript, we therefore investigate the domain structure of TRIOBP-1 and establish that such an aggregation-critical region exists, which can be narrowed down to a stretch of just 25 amino acids (aa), strongly supporting the idea that a specific mechanism exists by which TRIOBP-1 forms insoluble aggregates.

Results

Predicted coiled-coil structure of TRIOBP-1 and inclusion of its N-terminus – Previous predictions have suggested that TRIOBP-1 (RefSeq accession number NP_008963.3) contains a Pleckstrin homology (PH) domain near its N-terminus, while the majority of its C-terminal half forms α-helices, most likely in the form of coiled-coil domains (3). The potential coiled-coil composition of the C-terminal half of TRIOBP-1 was investigated theoretically using PSIPRED (14,15) and COILS (16) (Fig. 1A,B,C), with reference also to Paircoil2 (17). In this manner, we predicted the existence of six distinct putative coiled-coils (Fig. 1D) in human TRIOBP-1, which will be referred to as CC1-CC6. Of these, CC3, CC4 and CC5 are comparatively long stretches (running from approximately aa 395-465, aa 473-550 and aa 566-617 respectively), while CC1, CC2 and CC6 are shorter (aa 303-322, aa 352-372 and aa 623-642 respectively).

Note, that in this manuscript, the amino acids of human TRIOBP-1 are numbered based on a 652 aa long reading frame. This is 59 aa longer than the 593 aa reading frame considered in many other publications (3,10,11,18-20) as a result of the existence of two putative Kozak sequences and methionine residues at the 5' end of the *TRIOBP-1* transcript. Amino acid numbers quoted here for the 652 aa protein can therefore be converted to directly to positions in the 593 aa protein considered elsewhere by subtracting 59. We chose to include these additional 59 aa N-terminal region in the amino acid numbered as it is relatively well conserved and maintains its reading frame throughout mammalian species (Fig. 2A). Nevertheless, TRIOBP-1 species containing this region appear to represent a minority in cells (Fig. 2B) and therefore arise either from a less common translation event, or else they represent the approximate position of a

"pro" domain which is normally cleaved off in the cell. This 59 aa N-terminal region is rich in both prolines and positively charged residues and localizes to both the cytoplasm and nucleus when expressed in neuroblastoma cells (Fig. 2C).

The domain structure of TRIOBP-1 as determined by solubility and stability of recombinant protein fragments – In order to determine which regions have the potential to exist as distinct folded domains *in vivo*, different fragments of TRIOBP-1 were expressed as recombinant proteins. This was based on the premise that compactly folded protein domains are more likely to form soluble recombinant proteins, with distinct oligomeric states, both in bacteria and *in vitro*. In contrast, constructs encoding only part of such a region would instead be more likely to either degrade or form insoluble aggregates. In support of this idea, we began by investigating the strongly predicted PH domain at the N-terminus of TRIOBP-1. Expression of the whole PH domain (aa 60-189) led to a soluble recombinant protein which stably formed a dimer (apparent molecular weight, MW, ≈30 kDa, compared to a predicted MW of 17.3 kDa,) as analyzed by size exclusion chromatography (SEC, Fig. 3A). Circular dichroism (CD) analysis confirmed this protein to be structured, with a high β-sheet content, approximately 50% as predicted in DichroWeb using the CDSSTR method and SMP180 dataset (21-25), which is consistent with the typical structure of PH domains (Fig. 3B). In contrast, expression of a shorter construct lacking the N-terminal-most predicted β-strand of the PH domain (aa 93-189) led to an unstable recombinant protein. Specifically, the protein formed a high oligomeric state void volume species, excepting for a portion of the protein which instead broke down to yield a smaller soluble product (Fig. 3C).

Based on the principle that solubility and stability of a recombinant protein fragment *in vitro* can indicate the presence of distinct and complete folded domains *in vivo*, as exemplified here by the PH domain, the structure of the C-terminal half of TRIOBP-1 was investigated. When this whole coiled-coil region (aa 281-652) was expressed, it broke down within the bacteria into a number of discrete species (Fig. 4A & 4B), suggesting that the coiled coils region consists of at least two distinctly folded domains. Based on the sizes of the fragments detected with antibodies raised against different regions of the coiled coil region, a break between CC4 and CC5 was predicted. In agreement with this, expression of the extreme two C-terminal coiled coils of TRIOBP-1 (CC5 and CC6, aa 556-652) led to a single stable monomeric protein (Fig. 4C, observed MW ≈20 kDa, predicted MW: 14 kDa, discrepancy likely arising from coiled-coil protein forming an elongated structure), which has a predominantly α-helical structure as determined by CD (Fig. 4D). In contrast, inclusion of CC4 in the construct (CC4-CC6, aa 467-652) led to an unstable protein which broke down prior to purification (Fig. 4E). Together this implies that CC5-6 constitute a distinctly folded structure which we will refer to as the "C-terminal domain".

Expression of CC1-CC4 instead led to a predominant multimeric species with an apparent MW of approximately 200kDa (Fig. 5A, aa 281-555, predicted MW for a monomer: 34.2 kDa), suggestive of a hexamer. CD demonstrated it to be principally α-helical (Fig. 5B). This multimer was prone to precipitation at high concentrations, and there was some evidence of degradation of the protein (80-100ml in Fig. 5A, also visible in Fig. 6E), suggesting that this protein fragment was largely, but not completely, stable *in vitro*. A further truncated recombinant protein containing CC1-CC3 was highly stable even at concentrations of over 10 mg/ml, and existed as seemingly the same single oligomeric species as the CC1-CC4 protein (Fig.5C, aa 281-466, apparent MW: ≈160 kDa, predicted MW of a monomer: 24 kDa, again suggestive of a hexamer) and also had a high helical content (Fig. 5D). While these *in vitro* analyses may not necessarily completely reflect the situation *in vivo*, they strongly suggest that CC1-CC3 of TRIOBP-1 forms a folded "central domain", potentially also including CC4, but distinct from the C-terminal domain of CC5 & CC6.

When only the short CC1 & CC2 coiled regions were expressed, the ensuing protein appeared to be either a trimer or an extended dimer (Fig. 5E, aa 281-382, apparent MW: ≈40 kDa, predicted MW for a monomer: 14.1 kDa) and to be reasonably stable, although less so than the CC1-CC3 protein and with a lower α-helix content (Fig. 5F). Expression of CC2 & CC3 led to a similarly stable trimeric protein (Fig. 5G, aa 349-466, apparent MW: ≈55 kDa, predicted MW for a monomer: 16.2 kDa), which consisted almost entirely of α-helical structure (Fig 5H).

To further investigate the oligomeric state of the central domain, these constructs were

investigated using analytical ultracentrifugation (AUC). AUC sedimentation velocity experiments showed the CC1-CC2 fragment to exist predominantly as a species with an estimated MW of 26.0 kDa (Perrin factor, $s_{20,w}$ = 1.15 S, Fig. 6A,B), consistent with a dimer. It had a frictional ratio of 1.61, indicative of an extended conformation. Under the same experimental circumstances, most of the CC2-CC3 construct adopted an oligomeric state consistent with a monomer, only 1.8% of the protein remained as a species matching the one seen by SEC, with a predicted MW of 49.4 kDa ($s_{20,w}$ = 3.46 S, Fig. 6A,C). This region was even more elongated that CC1-CC2, with a frictional ratio of 1.82, consistent with it consisting of extended coiled coil structure. When CC1-CC3 was similarly examined, it did not maintain the same high order oligomeric state seen by SEC, with an apparent trimer being the largest species (observed MW of 76.3 kDa, compared to a theoretical MW of 23.9 kDa, Fig. 6A,D). This was also highly elongated (frictional ratio: 1.63). It therefore appears that the central domain trimerizes through interactions of CC2-CC3, but is also capable of forming higher order oligomers, most likely hexamers, through the additional dimer-forming capacity contained within CC1-CC2.

The nature of all soluble TRIOBP-1 constructs used here could be confirmed by Western blot using anti-TRIOBP antibodies raised against different sections of the protein (figure 6E).

Functional analysis of the individual domains of TRIOBP-1 – Following identification of two distinct coiled-coil domains of TRIOBP-1, in addition to the previously predicted PH domain, initial experiments were carried out to investigate their functions in the cell, the results of which are summarized in table 1.

The canonical role of TRIOBP-1 is as a modulator of actin polymerization, leading to increased fibular F-actin compared to globular G-actin (3), although the mechanism by which it does this so far has been unknown. The ability of the individual domains of TRIOBP-1 on actin polymerization was therefore investigated. NLF neuroblastoma cells were transfected with constructs encoding the PH domain, central domain (CC1-4) C-terminal domain (CC5-6) of TRIOBP-1 and lysed in a buffer which stabilizes polymerized F-actin (26). The ensuing lysates were then separated by ultracentrifugation into an F-actin containing pellet and a G-actin containing supernatant (Fig. 7A). The supernatant was incubated under conditions which promote polymerization, before being separated once again by ultra-centrifugation into F- and G-actin containing fractions, in order to determine how much of the G-actin had re-polymerized in the presence of each TRIOBP-1 construct. Similarly, the original F-actin containing pellet was resuspended and equilibrated in conditions which favor de-polymerization (27) and then separated by ultracentrifugation to determine what proportion of the polymeric F-actin had broken down into monomeric G-actin in the presence of each TRIOBP-1 construct (Fig. 7A).

The central (CC1-CC4) and C-terminal (CC5-CC6) domains of TRIOBP-1 were found to segregate with both F- and G-actin in the assay, while the PH domain was found exclusively in soluble fractions, implying that both coiled coil domains, but not the PH domain, can interact with F-actin (Fig. 7B). As would therefore be expected, the presence of the PH domain had no effect on the dynamics of actin in this assay, when compared to mock transfected control cells (Fig. 7B,C,D). The central domain had no effect on the polymerization of G-actin (Fig. 7B,D), but did cause an almost 3-fold reduction in the amount of F-actin which de-polymerized during the experimental time period (Fig. 7B,C). Expression of the C-terminal region was at a lower level than of the other two constructs, but nevertheless showed putative effects in limiting actin de-polymerization to the central domain (Fig. 7B,C), and in causing an increase in polymerization of G-actin (Fig. 7B,D), although neither of these remained significant after correction for multiple testing. We therefore demonstrate for the first time that the central domain, and potentially the C-terminal domain, but not the PH domain, is individually capable of interacting with F-actin and protecting it against de-polymerization, at least under these experimental conditions.

The exact role of TRIOBP-1 in neurons remains obscure, however over-expression of full length TRIOBP isoforms has been shown to influence neurite outgrowth (8). To determine which domain(s) could be involved in this process, Neuroscreen-1 cells were transfected with constructs encoding these domains, or an empty vector control, and then induced to differentiate for 72 hours with nerve growth factor. The morphology of the ensuing

transfected cells was then examined by immunofluorescent microscopy and quantified in a blinded manner (Fig. 8A). Notably, expression of the PH domain led to a significant increase of approximately 30% in the number of neurites per cell (Fig. 8B, only neurites over 20 μm in length were considered), suggesting this domain to play an active role in neurite initiation. There was also an increase in the length of the longest neurite per cell following expression of the PH domain, although this did not survive correction for multiple testing (Fig 8C). In contrast, expression of the central domain led to an approximately 30% decrease in neurite number relative to control cells (Fig 8B). The most likely explanation is that this is a dominant negative effect of expressing the actin-binding domain in isolation, and thus competing with endogenous TRIOBP-1. The C-terminal domain did not affect neurite outgrowth in this experiment.

The aggregation propensity of TRIOBP-1 is dependent on a 25 amino stretch between coiled coils 1 and 2 – In our previous paper, we found evidence that insoluble TRIOBP-1 may accumulate specifically in the brains of at least a subset of patients with schizophrenia (8). Furthermore, it was demonstrated that full length TRIOBP-1, or TRIOBP-1 lacking its PH domain, can be made to aggregate when over-expressed in neuroblastoma cells, thus providing a potential model for insoluble TRIOBP-1 in the brain (8). Similar aggregated accumulations of exogenously expressed TRIOBP-1 have also recently been reported by others (28). If the aggregation propensity of TRIOBP-1 arises as a result of a specific cellular mechanism, such as being modulated by a protein-protein interaction or post-translational modification, then it should be possible to identify a specific region of TRIOBP-1 which is critical for this aggregation event to occur. To investigate this, further constructs encoding fragments of TRIOBP-1 were generated, this time fused to N-terminal Flag tags, and were expressed in human SH-SY5Y neuroblastoma cells.

Notably, while full length TRIOBP-1 forms aggregates when over-expressed (Fig. 9A), the N-terminal region of TRIOBP-1 showed no such tendency, instead being found in the cytoplasm and at the periphery of the cell, where it co-localized with actin (aa 1-280, Fig. 9B). When the PH domain was expressed in isolation it showed a similar cell periphery/actin localization with no sign of aggregation, but was also found prominently in the nucleus (aa 60-189, Fig. 9C). This was in agreement with our previous finding that deleting the PH domain of TRIOBP-1 did not ablate its aggregation propensity (8).

In contrast, a construct encoding CC1-CC6 of TRIOBP-1 was seen to form large accumulations in the cell (aa 281-652, Fig. 9D), as did a construct encoding just CC1-CC4, the central domain (281-555 Fig. 9E). Reinforcing that the aggregation propensity of TRIOBP-1 arises from the central domain, the C-terminal domain alone formed a diffuse cytoplasmic pattern when the two coiled coil regions of this domain were expressed (CC5 & CC6, aa 556-652, Fig. 9F), or when CC5 was expressed alone (aa 556-619, Fig. 9G).

In order to determine which section of the TRIOBP-1 central coiled domain was involved in aggregation, further truncation constructs were expressed in neuroblastoma cells. Notably, neither constructs containing only CC3-6, nor CC3-4 formed aggregates (aa 383-652 and aa 383-555, Fig. 10A & 10B), implying that an aggregation-critical region or motif lies within the first two short coiled-coils. CC1 and CC2 alone were unstable and rapidly degraded when expressed in the cell, but could be stabilized by the addition of a CFP fusion protein (Fig. 10C). Alone, this region did not show clear aggregation, which was not a quenching effect of the CFP, as full length TRIOBP-1 fused to CFP formed clear aggregates (Fig. 10D). Instead, fine mapping of the aggregation critical region was performed by systematic removal of sections of the CC1-CC6 construct from the N-terminal end. Two constructs expressing CC2-CC6 were therefore generated, one incorporating a 25 aa stretch which lies between CC1 and CC2, and one lacking this short section. Dramatically, while the construct featuring this region formed aggregates (aa 324-652, Fig. 10E), the protein lacking it instead adopted a more natural cytoplasmic expression pattern (aa 349-652, Fig. 10F).

To determine whether these punctate structures really represented insoluble TRIOBP-1 species, both constructs were expressed in cells which, after lysis, were subjected to a series of solubilization buffers and centrifugation steps in order to remove all but the most insoluble proteins. Upon examination by western blot, both the constructs encoding aa 324-652 and aa 349-652 were seen to be present in cell lysates, but only 324-652 was retained in the insoluble

protein fraction (Fig. 11A), consistent with its representing an insoluble, aggregated TRIOBP-1 species. This 25 aa "linker" region between CC1 and CC2 therefore appears to be critical for its aggregation propensity. To further verify this, SH-SY5Y cells were transfected with five previously-employed TRIOBP-1 truncation constructs in a blinded manner and the number of TRIOBP aggregates per cell was quantified. The presence of this 25 aa region was shown to have a highly significant effect on the number of such aggregates in the cytoplasm (Fig. 11B), with three constructs containing the region having a mean of at least 1.3 aggregates per cell, compared to 0.1 or less for two constructs lacking this region. This therefore reinforces the idea that this subsection of the coiled central region is essential for aggregation. Amongst the cells displaying TRIOBP-1 aggregates (which for the purposes of this experiment were defined as any intense area of anti-Flag signal over 0.5 μm in diameter in the cell body) there was variation in the size of TRIOBP-1 aggregate seen, but with no significant differences between the different TRIOBP-1 fragments used (Fig. 11C).

When tested by Western blot, there was some variation in the level of expression of proteins from these construct (Fig. 11D), likely representing variable levels of nonsense-mediated decay, however there was no obvious correlation (positive or negative) between expression level and aggregation propensity.

To further confirm the requirement of this region for aggregation, long TRIOBP-1 constructs containing the entire coiled-coil region (aa 190-652, Fig. 11E) were confirmed to aggregate when expressed in SH-SY5Y, but not when this 25 aa region was deleted (aa 190-652 Δ324-348, Fig. 11F). Note that these fragments could not be readily studied by SEC as, like the aa 281-652 construct (Fig 4A,B), they degraded into smaller stable fragments when purified from bacteria. The N-terminal region plus CC1-2 did not aggregate however (aa 1-382, Fig. 11G), demonstrating that while this 25 aa "linker" region is essential for aggregation to occur, it is not in itself sufficient to induce aggregation, requiring the presence of at least some other part of the central domain. The reason for this lack of aggregation is likely due to loss of a more C-terminal section of TRIOBP-1, rather than a stabilizing effect of the PH domain, given that full length TRIOBP-1 aggregates (Fig. 9A, 10D) and previous experiments have shown that deletion of the PH domain has no effect on aggregation propensity (8).

Discussion

Many chronic neurodegenerative conditions can be characterized by the presence of insoluble aggregates of specific proteins as evidence for aberrant proteostasis. The concept that aberrant proteostasis may also exist in psychiatric illness is an emerging one, with TRIOBP-1 being a potential example of such a protein, having been identified via a hypothesis-free affinity proteomics approach using brain samples of patients with schizophrenia (8).

Here, we have demonstrated that a specific region of TRIOBP-1, bounded by aa 324-348, is an absolute requirement for its aggregation, indicating that it is likely to occur through a specific physiological process, as opposed to the random aggregation of naturally "sticky" proteins. This was revealed through the expression of truncated TRIOBP-1 constructs in neuroblastoma cell lines. While these truncated forms of TRIOBP-1 are not believed to be expressed *in vivo*, their similarity in expression pattern to full length TRIOBP-1 suggests that they may nevertheless be a useful tool to study its protein aggregation. This 25 aa region lies between two short predicted coiled-coils, CC1 and CC2 (Fig. 12A), which form a dimeric structure when expressed in isolation, but appear to be part of the larger hexameric central coiled coil domain. In our previous analyses (8), this portion of TRIOBP-1 was one of the less strongly predicted to contain an "aggregation motif", with only the sequence around aa 230-236 being predicted to have some aggregate-forming propensity by the AGGRESCAN (29), FoldAmyloid (30) and ProA (31) servers. It was nor predicted as such by TANGO (32,33). In all instances, however, at least four sites elsewhere in the protein were more strongly predicted to be capable of inducing aggregation, thus this location for an aggregation-critical region was an unexpected result. The 25 aa region contains multiple proline residues (Fig. 12B), suggesting that it likely represents a turn between CC1 and CC2. It is also rich in charged amino acids, allowing for the possibility that TRIOBP-1 aggregation is dependent on protein-protein interactions, of which several have previously been reported for TRIOBP-1 (3,18,19). That this region was not strongly predicted to have an innate aggregation propensity might further

implicate the involvement of additional proteins or other cellular factors in the aggregation process, with such factors instead interacting with TRIOBP-1 in a manner dependent on this 25 aa region.

The large size of the protein aggregates generated when TRIOBP-1 constructs incorporating this region were expressed, combined with the high variability in the sizes of this protein accumulations, are consistent with their consisting of unfolded or misfolded TRIOBP-1 species. The exact mechanism by which TRIOBP-1 aggregation occurs remains to be determined, but it is likely to be tied into its oligomeric state and/or its protein interaction partners. An E3 ubiquitin ligase, HECTD3 (Homologous to E6-AP Carboxyl Terminus protein D3) has also been reported to be responsible for degradation of TRIOBP-1 (19), and it is therefore likely that disruption of this process could lead to aberrant TRIOBP-1 protein homeostasis, potentially including aggregation.

We have also more generally explored the domain organization of TRIOBP-1, which was strongly predicted to consist of an N-terminal PH domain and a large C-terminal coiled-coil region. The predicted PH domain is now confirmed to be a distinctly folded region when expressed *in vitro*, and appears to be of functional relevance for the generation of neurites based on a neuron-like assays in cell culture. Furthermore, we have now found the coiled-coil region to consist of two distinct domains: the central domain consisting of CC1-CC3, and potentially also of CC4, while the C-terminal domain consists of CC5-CC6 (Fig. 11A). The central region is responsible for the assembly of TRIOBP-1 oligomers, forming an oligomeric state comparable to that previously described for the full length protein (18), and containing the aggregation-critical region. CC4 corresponds to the region of TRIOBP-1 recently identified to be required for interaction with NDEL1 and subsequent effects on cell migration (11) and also contains a known phosphorylation site of importance for mitotic progression (10). The central domain is also involved in neurite outgrowth, with its expression in isolation leading to a reduction in neurite number, possibly as a result of the truncation mutant having a dominant negative effect.

That expression of TRIOBP-1 leads to an increase in cellular polymerized F-actin is well established (3), and knockdown of TRIOBP-1 can be used as a tool to prevent F-actin formation in the cell (9,34), however the mechanism by which it does this is unclear. Here we demonstrate that, at least when expressed in isolation, both the central and C-terminal domains can bind to F-actin, with the central domain limiting its de-polymerization. The C-terminal domain also showed a trend towards the same effect. These data suggest that the TRIOBP-1 protein promotes F-actin formation indirectly, by inhibiting its degradation into monomeric G-actin This is broadly in agreement with previous results showing that amino acids 72-444 of TRIOBP-1 (adapted to the numbering system used here, and incorporating the PH domain plus approximately CC1-3) are sufficient to bind actin (3). That the central and C-terminal domains are each capable of modulating actin dynamics in isolation is analogous to the fact that both the TRIOBP-1 and TRIOBP-4 proteins modulate actin despite sharing no common amino acid sequence. It thus appears that longer isoforms of TRIOBP, such as TRIOBP-6, could contain at least three distinct actin-binding and modulating domains: the central and C-terminal regions of TRIOBP-1, plus the R1 motif of TRIOBP-4 (5).

To the best of our knowledge, four other proteins have so far been identified which may also form protein aggregates in mental illness. Of these, both DISC1 (Disrupted in Schizophrenia 1) and dysbindin-1B are proteins encoded for by genetic risk factors for major mental illness, which were later found in insoluble protein fractions of subsets of patients with mental illness (35,36). CRMP1 (Collapsin Response Mediator Protein 1) was identified through a combination of genetics and our antibody-based proteomics approach (6), while NPAS3 (Neuronal PAS domain protein 1) aggregation appears to occur in the presence of a point mutation which is found in a family with schizophrenia (37,38). In all these cases, like TRIOBP-1, over-expression of the protein in mammalian cells leads to the formation of protein aggregates (6,36,38), and in the case of DISC1 and dysbindin-1B this has also be seen in when transgenic human proteins are expressed in rodents (39-41). NPAS3 aggregation, like that of TRIOBP-1 appears to be dependent on a particular region of the protein, in this case narrowed to an approximately 100 aa long region

which including the aggregation-related point mutation (38). While such experiments have not been directly undertaken for the other proteins, early work on DISC1 did describe a central region of the protein as required for its subcellular localization to "puncta" (42) reminiscent of protein aggregates. Furthermore, a seemingly distinct region of the C-terminus has been shown to be responsible for the aggregation propensity of recombinant DISC1 proteins (43).

TRIOBP-1 is therefore one of several proteins which appear to form aggregates in cell culture systems through specific, although not yet elucidated, cellular processes, and which are also implicated in forming insoluble complexes in the brain. If, as we would predict, these insoluble accumulations in the brain correspond in form and effect to the aggregated protein structures seen in cell culture systems, then further study of such aggregates would yield significant insight into the pathophysiological events underlying chronic mental illness.

Experimental procedures

Plasmid constructs - The human TRIOBP-1 652 aa open reading frame (RefSeq accession number NP_008963.3) was cloned from the cDNA of human SH-SY5Y neuroblastoma cells and then regions of the gene were subcloned. These reading frames were transferred into the pDONR/Zeo vector using BP clonase (plasmid and enzyme from Thermo Fischer Scientific, Darmstadt, Germany), except for the full-length protein which was cloned and ligated into the pENTR1A no ccDB vector (44) (E. Campeau, #17298, Addgene, Cambridge, MA, USA). These reading frames were then transferred using LR clonase II (Thermo Fischer Scientific) into one or more of the following destination vectors: pETG10A (A. Geerlof, EMBL, Heidelberg, Germany), pdcDNA-FlagMyc (B. Janssens, #LMBP 4705, BCCM/LMBP Plasmid Collection, Zwijnaarde, Belgium) or pdECFP (45) (S. Wiemann, #LMBP 4548, BCCM/LMBP Plasmid Collection). All constructs were confirmed by sequencing, and the expressed proteins confirmed by western blot.

Recombinant protein expression and purification - Recombinant TRIOBP-1 fragments were expressed from pETG10A vectors in BL21 Star (DE3) or Rosetta (DE3) pLysS *E. coli* (respectively from Thermo Fisher Scientific and Merck Millipore, Darmstadt, Germany) and induced with 0.2-1 mM IPTG under conditions optimized for each construct. Bacterial pellets were resuspended in 20 mM Tris pH 7.4, 500 mM NaCl, 25 mM imidazole, 20 mM $MgCl_2$ containing protease inhibitors and DNaseI, and lysed by the addition of 1 mg/ml lysozyme and 1% Triton X-100. Insoluble material was removed by centrifugation, and the soluble fraction incubated for 16 hours at 4^0C with NTA-agarose resin (Qiagen, Hilden, Germany). Resin was then transferred to a gravity flow column and washed with 20 mM Tris pH 7.4, 500mM NaCl, 25 mM imidazole. Protein was eluted by the addition of the same buffer containing 250 mM imidazole. Further purification was performed by SEC on a HiLoad 16/600 Superdex 200pg column (GE Healthcare, Freiburg, Germany), pre-equilibrated with 20 mM Tris pH 7.4, 150 mM NaCl. This was performed using an ÄKTA Pure system (GE Healthcare) which was kept cooled to 4-8 ^{0}C at all times. Inferred molecular weights of protein peaks were calculated based on calibration with protein standards, and compared to theoretical molecular weights calculated using the ExPASy ProtParam tool (46). For CD and AUC analyses, proteins were transferred to 20 mM sodium phosphate pH 7.4, 150 mM sodium fluoride using a HiPrep 26/10 Desalting column (GE Healthcare).

Circular dichroism – Protein samples were analyzed on a J-815 spectrometer (JASCO, Groß-Umstadt, Germany). Measurements were recorded at λ = 260 nm to 185 nm, using a 1 nm resolution, 20 nm/min scan speed, 1 mm optical path length, an integration time of 0.5 s and a controlled temperature of 20 °C. An average reading was taken from ten spectra per experiment. A buffer only spectra was subtracted from these results, and the data was then transformed to units of mean residue ellipticity. Deconvolution of the data was performed in DichroWeb (21,22) using the CDSSTR method (23,24) and reference dataset SMP180 (25).

Analytical Ultracentrifugation – Measurements were carried out using a Beckman Optima XL-A ultracentrifuge (Beckman-Coulter, Brea, CA, USA) equipped with an absorbance detector and an 8-hole rotor. For sedimentation velocity experiments, 400 µL samples were loaded into a 12 mm double-sector aluminum

cell. All samples were equilibrated to 20 °C and the centrifugation was performed at 20 °C at 50,000 rpm. The absorbance readings of all samples were recorded at 285 nm with a radial resolution of 30 μm. Data were analyzed by Sedfit (version 15.01b) using the continuous c(*s*) distribution model. The partial specific volumes of the target proteins, buffer density and its viscosity were determined by Sednterp (version 20130813BETA). All graphs were generated by GUSSI (version 1.2.1) and the reported *s*-values were normalized to $s_{20,w}$ -values.

Western blot, gels and quantification - Acrylamide gels were run, transferred to nitrocellulose membranes and blocked according to standard protocols. Commercial antibodies were used against α-actin (#A2066, Sigma-Aldrich, Munich, Germany, raised in rabbit) the Flag tag (#F1804, Sigma-Aldrich, raised in mouse), the 6xHis tag (#27E8, Cell Signaling Technology, Danvers, MA, USA, raised in mouse), TRIOBP-1 (#SAB2102579, #HPA019769 and #HPA003747, Sigma-Aldrich, raised in rabbit against human TRIOBP-1 recombinant protein fragments containing amino acids 144-193, 279-379 and 504-635 respectively) and α-tubulin (#T9026, Sigma-Aldrich, raised in rabbit). Antibody signal was visualized and quantified where necessary using IRDye secondary antibodies, an Odyssey Clx instrared imaging system and associated analysis software (LI-COR Biosciences, Bad Homburg, Germany). Total protein in acrylamide gels was visualized using InstantBlue (Expedeon, Swavesey, UK).

Cell culture - The human neuroblastoma cell line SH-SY5Y (Leibniz Institute DMSZ, Braunshweig, Germany) was cultured in D-MEM/F-12 containing 10% fetal calf serum, 1x MEM non-essential amino acids, penicillin and streptomycin. The human neuroblastoma cell line NLF (Children's Hospital of Philadelphia, PA, USA) were grown in RPM1 1640 medium supplemented with 10% fetal calf serum, 2 mM L-glutamine, penicillin and streptomycin. The rat pheochromocytoma cell line Neuroscreen-1 (Thermo Fischer Scientific) was grown in RPM1 1640 medium supplemented with 10% horse serum, 5% fetal calf serum, 2 mM L-glutamine, penicillin and streptomycin. Transfections were performed for 24 hours using Lipofectamine 2000 according to manufacturers' instructions. For neurite outgrowth experiments, Neuroscreen-1 cells were given 50 ng/ml nerve growth factor for 72 hours, following transfection. All cell culture chemicals from Thermo Fischer Scientific. Cells expressing full length TRIOBP-1 in a doxycycline-inducible manner were established using the Retro-X Tet-On Advanced Inducible Expression System (Clontech Laboratories, Mountain View, CA, USA).

Immunocytochemistry - Cells were seeded on glass coverslips, fixed with PBS, 4% paraformaldehyde, permeabilized with PBS, 0.5% Triton X-100 and blocked with PBS, 10% goat serum. Primary antibodies were applied and detected using Alex Fluor secondary antibodies (488 or 596 nm, Thermo Fischer Scientific). Actin was visualized using Acti-stain 488 phalloidin (#PHDG1, Cytoskeleton, Inc., Denver, CO, USA) according to manufacturer's instructions. This was also used to visualize total cell body and neurites in quantification experiments. Coverslips were mounted using ProLong Gold with DAPI (Thermo Fischer Scientific) and viewed on an LSM-510 confocal microscope (Carl Zeiss Microscopy, Göttingen, Germany) at room temperature. Images were taken using a Plan-Apochromat x100 objective, Immersol 518 immersion oil and ZEN 2 pro software (all from Carl Zeiss Microscopy). All images displayed are representative of at least three independent experiments.

For the quantification experiments, plasmid DNA preparations were prepared and then coded, so that the researcher performing transfections and immunocytochemistry was blinded as to which TRIOBP-1 construct was used for each set of cells. Photographs were then taken of the first transfected cells identified by microscopy, and quantified measurements taken from these images (using ImageJ, version 1.45s,(47)) prior to unblinding of the samples. Data was analyzed by one-way ANOVA, with Bonferroni correction for multiple testing.

Insoluble protein fraction purification - Purification of the insoluble fractions of SHSY-5Y cells was performed as described previously (8). Briefly, cells were lysed and washed with a series of buffers, variously containing 1% NP-40, 0.2% Sarcosyl, DNaseI and/or 1.5 M NaCl, with centrifugation steps to remove all proteins solubilized by each buffer. The final pellet was then resuspended in loading buffer and probed

by western blot alongside samples of the original, unfractionated cell lysate.

Actin polymerization assays – NLF neuroblastoma cells were transfected with constructs encoding regions of TRIOBP-1, or an empty control vector, and grown for 48 hours. Cells were then lysed at 37 °C with 50 mM PIPES pH 6.9, 50 mM NaCl, 5 mM $MgCl_2$, 5 mM EGTA, 5% glycerol, 0.1% NP-40, 0.1% Triton X-100, 1% Tween 20 plus protease inhibitor cocktail for 10 minutes with gentle shaking. Cell debris was removed by centrifuging at 350 × g for 10 mins. Cell lysate was then ultracentrifuged at 100,000 × g for 1 hour at 37 °C and the G-actin containing supernatant removed. The supernatant was incubated for a further 60 mins at 37 °C and then ultracentrifuged again to test for additional polymerization of actin. Meanwhile, the F-actin containing pellet was resuspended in 5 mM Tris pH 8.0, 0.2 mM $CaCl_2$, 0.2 mM ADP plus protease inhibitor cocktail. This was incubated for 4 hours at 4 °C to facilitate de-polymerization of actin, and then ultracentrifuged at 100,000 × g for 1 hour at 4 °C. Pellets from this second round of ultracentrifugation were resuspended in their respective buffers. Actin and TRIOBP-1 content was assayed by western blot. Experiment was repeated three times.

Author contributions – NJB designed and performed experiments, except for the circular dichroism and analytical centrifugation experiments, which were designed by LN-S and performed by ASKY and TZ. NJB and RM generated novel reagents. NJB and CK wrote the paper, with input from the other authors. All authors analyzed the results and approved the final version of the manuscript.

Acknowledgments – This work was funded by the Fritz Thyssen Stiftung (10.14.2.140 to NJB), the Heinrich Heine University, Düsseldorf (graduate school "iBrain" to CK and grant 9772547 from the Forschungskommission der Medizinischen Fakultät to NJB), the EU Seventh Framework Program (MC-IN "IN-SENS" #60761 to CK) and the Brain Behavior Research Foundation (NARSAD Independent Investigator Award #20350 to CK).

Conflict of interest - The authors declare that they have no conflicts of interest with the contents of this article.

References

1. Riazuddin, S., Khan, S. N., Ahmed, Z. M., Ghosh, M., Caution, K., Nazli, S., Kabra, M., Zafar, A. U., Chen, K., Naz, S., Antonellis, A., Pavan, W. J., Green, E. D., Wilcox, E. R., Friedman, P. L.*, et al.* (2006) Mutations in *TRIOBP,* which encodes a putative cytoskeletal-organizing protein, are associated with nonsyndromic recessive deafness. *Am. J. Hum. Genet.* **78**, 137-143
2. Shahin, H., Walsh, T., Sobe, T., Abu Sa'ed, J., Abu Rayan, A., Lynch, E. D., Lee, M. K., Avraham, K. B., King, M.-C., and Kanaan, M. (2006) Mutations in a novel isoform of TRIOBP that encodes a filamentous-actin binding protein are responsible for DFNB28 recessive nonsyndromic hearing loss. *Am. J. Hum. Genet.* **78**, 144-152
3. Seipel, K., O'Brien, S. P., Iannotti, E., Medley, Q. G., and Streuli, M. (2001) Tara, a novel F-actin binding protein, associates with the Trio guanine nucleotide exchange factor and regulates actin cytoskeletal organization. *J. Cell Sci.* **114**, 389-399
4. Kitajiri, S.-i., Sakamoto, T., Belyantseva, I. A., Goodyear, R. J., Stepanyan, R., Fujiwara, I., Bird, J. E., Riazuddin, S., Riazuddin, S., Ahmed, Z. M., Hinshaw, J. E., Sellers, J., Bartles, J. R., Hammer, J. A., Richardson, G. P.*, et al.* (2010) Actin-bundling protein TRIOBP forms resilient rootlets of hair cell stereocilia essential for hearing. *Cell* **141**, 786-798
5. Bao, J., Bielski, E., Bachhawat, A., Taha, D., Gunther, L. K., Thirumurugan, K., Kitajiri, S.-i., and Sakamoto, T. (2013) R1 motif is the major actin-binding domain of TRIOBP-4. *Biochemistry* **52**, 5256-5264
6. Bader, V., Tomppo, L., Trossbach, S. V., Bradshaw, N. J., Prikulis, I., Leliveld, S. R., Lin, C.-Y., Ishizuka, K., Sawa, A., Ramos, A., Rosa, I., García, Á., Requena, J. R., Hipolito, M., Rai, N.*, et al.* (2012) Proteomic, genomic and translational approaches identify CRMP1 for a role in schizophrenia and its underlying traits. *Hum. Mol. Genet.* **21**, 4406-4418

7. Korth, C. (2012) Aggregated proteins in schizophrenia and other chronic mental diseases: DISC1opathies. *Prion* **6**, 134-141
8. Bradshaw, N. J., Bader, V., Prikulis, I., Lueking, A., Müllner, S., and Korth, C. (2014) Aggregation of the protein TRIOBP-1 and its potential relevance to schizophrenia. *PLOS One* **9**, e111196
9. Lee, S. H., Lee, Y. J., Park, S. W., Kim, H. S., and Han, H. J. (2011) Caveolin-1 and Integrin β1 regulate embryonic stem cell proliferation via p38 MAPK and FAK in high glucose. *J. Cell. Physiol.* **226**, 1850-1859
10. Zhu, Y., Wang, C., Lan, J., Yu, J., Jin, C., and Huang, H. (2012) Phosphorylation of Tara by Plk1 is essential for faithful chromosome segregation in mitosis. *Exp. Cell Res.* **318**, 2344-2352
11. Hong, J.-H., Kwak, Y., Woo, Y., Park, C., Lee, S.-A., Lee, H., Park, S. J., Suh, Y., Suh, B. K., Goo, B. S., Mun, D. J., Sanada, K., Nguyen, M. D., and Park, S. K. (2016) Regulation of the actin cytoskeleton by the Ndel1-Tara complex is critical for cell migration. *Sci. Rep.* **6**, 31827
12. Bradshaw, N. J., and Hayashi, M. A. F. (2017) NDE1 and NDEL1 from genes to (mal)functions: Parallel but distinct roles impacting on neurodevelopmental disorders and psychiatric illness. *Cell. Mol. Life Sci.* **74**, 1191-1210
13. Maycox, P. R., Kelly, F., Taylor, A., Bates, S., Reid, J., Logendra, R., Barnes, M. R., Larminie, C., Jones, N., Lennon, M., Davies, C., Hagan, J. J., Scorer, C. A., Angelinetta, C., Akbar, T.*, et al.* (2009) Analysis of gene expression in two large schizophrenia cohorts identifies multiple changes associated with nerve terminal function. *Mol. Psychiatry* **14**, 1083-1094
14. Jones, D. T. (1999) Protein secondary structure prediction based on position-specific scoring matrices. *J. Mol. Biol.* **292**, 195-202
15. Buchan, D. W. A., Minneci, F., Nugent, T. C. O., Bryson, K., and Jones, D. T. (2013) Scalable web services for the PSIPRED Protein Analysis Workbench. *Nucl. Acids Res.* **41**, W349-357
16. Lupas, A., Van Dyke, M., and Stock, J. (1991) Predicting coiled coils from protein sequences. *Science* **252**, 1162-1164
17. McDonnell, A. V., Jiang, T., Keating, A. E., and Berger, B. (2006) Paircoil2: improved prediction of coiled coils from sequence. *Bioinformatics* **22**, 356-358
18. Li, X., Lan, J., Zhu, Y., Yu, J., Dou, Z., and Huang, H. (2007) Expression, purification, and characterization of Tara, a novel telomere repeat-binding factor 1 (TRF1)-binding protein. *Protein Expr. Purif.* **55**, 84-92
19. Yu, J., Lan, J., Zhu, Y., Li, X., Lai, X., Xue, Y., Jin, C., and Huang, H. (2008) The E3 ubiquitin ligase HECTD3 regulates ubiquitination and degradation of Tara. *Biochem. Biophys. Res. Commun.* **367**, 805-812
20. Yano, T., Yamazaki, Y., Adachi, M., Okawa, K., Fort, P., Uji, M., Tsukita, S., and Tsukita, S. (2011) Tara up-regulates E-cadherin transcription by binding to the Trio RhoGEF and inhibiting Rac signaling. *J. Cell Biol.* **193**, 319-332
21. Whitmore, L., and Wallace, B. A. (2004) DICHROWEB, an online server for protein secondary structure analyses from circular dichroism spectroscopic data. *Nucl. Acids Res.* **32**, W668-W673
22. Whitmore, L., and Wallace, B. A. (2008) Protein secondary structure analyses from circular dichroism spectroscopy: Methods and reference databases. *Biopolymers* **89**, 392-400
23. Manavalan, P., and Johnson Jr, W. C. (1987) Variable selection method improves the prediction of protein secondary structure from circular dichroism spectra. *Anal. Biochem.* **167**, 76-85
24. Sreerama, N., and Woody, R. W. (2000) Estimation of protein secondary structure from circular dichroism spectra: Comparison of CONTIN, SELCON, and CDSSTR methods with an expanded reference set. *Anal. Biochem.* **287**, 252-260
25. Abdul-Gader, A., Miles, A. J., and Wallace, B. A. (2011) A reference dataset for the analyses of membrane protein secondary structures and transmembrane residues using circular dichroism spectroscopy. *Bioinformatics* **27**, 1630-1636

26. Cenni, V., Sirri, A., Riccio, M., Lattanzi, G., Santi, S., de Pol, A., Maraldi, N. M., and Marmiroli, S. (2003) Targeting of the Akt/PKB kinase to the actin skeleton. *Cell. Mol. Life Sci.* **60**, 2710-2720
27. Tamura, M., Ito, K., Kunihiro, S., Yamasaki, C., and Haragauchi, M. (2011) Production of human β-actin and a mutant using a bacterial expression system with a cold shock vector. *Protein Expr. Purif.* **78**, 1-5
28. Kazmierczak, M., Kazmierczak, P., Peng, A. W., Harris, S. L., Shah, P., Puel, J.-L., Lenoir, M., Franco, S. J., and Schwander, M. (2017) Pejvakin, a candidate stereociliary rootlet protein, regulates hair cell function in a cell-autonomous manner. *J. Neurosci.* **doi:10.1523/JNEUROSCI.2711-16.2017**
29. Conchillo-Solé, O., de Groot, N. S., Avilés, F. X., Vendrell, J., Daura, X., and Ventura, S. (2007) AGGRESCAN: a server for the prediction and evaluation of "hot spots" of aggregation in polypeptides. *BMC Bioinformatics* **8**, 65
30. Garbuzynskiy, S. O., Lobanov, M. Y., and Galzitskaya, O. V. (2010) FoldAmyloid: a method of prediction of amyloidogenic regions from protein sequence. *Bioinformatics* **26**, 326-332
31. Fang, Y., Gao, S., Tai, D., Middaugh, C. R., and Fang, J. (2013) Identification of properties important to protein aggregation using feature selection. *BMC Bioinformatics* **14**, 314
32. Fernandez-Escamilla, A.-M., Rousseau, F., Schymkowitz, J., and Serrano, L. (2004) Prediction of sequence-dependent and mutational effects on the aggregation of peptides and proteins. *Nat Biotech* **22**, 1302-1306
33. Linding, R., Schymkowitz, J., Rousseau, F., Diella, F., and Serrano, L. (2004) A comparative study of the relationship between protein structure and β-aggregation in globular and intrinsically disordered proteins. *J. Mol. Biol.* **342**, 345-353
34. Lee, Y. J., Kim, M. O., Ryu, J. M., and Han, H. J. (2012) Regulation of SGLT expression and localization through Epac/PKA-dependent caveolin-1 and F-actin activation in renal proximal tubule cells. *Biochim. Biophys. Acta* **1823**, 971-982
35. Leliveld, S. R., Bader, V., Hendriks, P., Prikulis, I., Sajnani, G., Requena, J. R., and Korth, C. (2008) Insolubility of Disrupted-in-Schizophrenia 1 disrupts oligomer-dependent interactions with Nuclear Distribution Element 1 and is associated with sporadic mental disease. *J. Neurosci.* **28**, 3839-3845
36. Ottis, P., Bader, V., Trossbach, S. V., Kretzschmar, H., Michel, M., Leliveld, S. R., and Korth, C. (2011) Convergence of two independent mental disease genes on the protein level: Recruitment of dysbindin to cell-invasive Disrupted-in-Schizophrenia 1 aggresomes. *Biol. Psychiatry* **70**, 604-610
37. Yu, L., Arbez, N., Nucifora, L. G., Sell, G. L., DeLisi, L. E., Ross, C. A., Margolis, R. L., and Nucifora, F. C. (2014) A mutation in NPAS3 segregates with mental illness in a small family. *Mol. Psychiatry* **19**, 7-8
38. Nucifora, L. G., Wu, Y. C., Lee, B. J., Sha, L., Margolis, R. L., Ross, C. A., Sawa, A., and Nucifora Jr, F. C. (2016) A mutation in NPAS3 that segregates with schizophrenia in a small family leads to protein aggregation. *Mol. Neuropsychiatry* **2**, 133-144
39. Trossbach, S. V., Bader, V., Hecher, L., Pum, M. E., Masoud, S. T., Prikulis, I., Schäble, S., de Souza Silva, M. A., Su, P., Boulat, B., Chwiesko, C., Poschmann, G., Stühler, K., Lohr, K. M., Stout, K. A.*, et al.* (2016) Misassembly of full-length Disrupted-in-Schizophrenia 1 protein is linked to altered dopamine homeostasis and behavioral deficits. *Mol. Psychiatry* **21**, 1561-1572
40. Zhu, C.-Y., Shen, Y., and Xu, Q. (2015) Propagation of dysbindin-1B aggregates: exosome-mediated transmission of neurotoxic deposits. *Neuroscience* **291**, 301-316
41. Yang, W., Zhu, C., Shen, Y., and Xu, Q. (2016) The pathogenic mechanism of dysbindin-1B toxic aggregation: BLOC-1 and intercellular vesicle trafficking. *Neuroscience* **333**, 78-91
42. Brandon, N. J., Schurov, I., Camargo, L. M., Handford, E. J., Duran-Jimeriz, B., Hunt, P., Millar, J. K., Porteous, D. J., Shearman, M. S., and Whiting, P. J. (2005) Subcellular targetting of DISC1 is dependant on a domain independent from the Nudel binding site. *Mol. Cell. Neurosci.* **28**, 613-624
43. Leliveld, S. R., Hendriks, P., Michel, M., Sajnani, G., Bader, V., Trossbach, S., Prikulis, I., Hartmann, R., Jonas, E., Willbold, D., Requena, J. R., and Korth, C. (2009) Oligomer

assembly of the C-terminal DISC1 domain (640-854) is controlled by self-association motifs and disease-associated polymorphism S704C. *Biochemistry* **48**, 7746-7755
44. Campeau, E., Ruhl, V. E., Rodier, F., Smith, C. L., Rahmberg, B. L., Fuss, J. O., Campisi, J., Yaswen, P., Cooper, P. K., and Kaufman, P. D. (2009) A versatile viral system for expression and depletion of proteins in mammalian cells. *PLOS One* **4**, e6529
45. Simpson, J. C., Wellenreuther, R., Poustka, A., Pepperkok, R., and Wiemann, S. (2000) Systematic subcellular localization of novel proteins identified by large-scale cDNA sequencing. *EMBO Rep.* **1**, 287-292
46. Gasteiger, E., Hoogland, C., Gattiker, A., Duvaud, S., Wilkins, M. R., Appel, R. D., and Bairoch, A. (2005) Protein identification and analysis tools on the ExPASy server. in *The Proteomics Protocols Handbook* (Walker, J. M. ed.), Humana Press Inc., Totowa, NJ. pp 571-607
47. Schneider, C. A., Rasband, W. S., and Eliceiri, K. W. (2012) NIH Image to ImageJ: 25 years of image analysis. *Nat Meth* **9**, 671-675
48. Sievers, F., Wilm, A., Dineen, D., Gibson, T. J., Karplus, K., Li, W., Lopez, R., McWilliam, H., Remmert, M., Söding, J., Thompson, J. D., and Higgins, D. G. (2011) Fast, scalable generation of high-quality protein multiple sequence alignments using Clustal Omega. *Mol. Syst. Biol.* **7**, 539

Abbreviations

aa: Amino acid, AUC: Analytical ultracentrifugation, CC: Coiled-Coil, CD: Circular dichroism, CRMP1: Collapsin Response Mediated Protein 1, DISC1: Disrupted in Schizophrenia 1, HECTD3: Homologous to E6-AP Carboxyl Terminus protein D3, IPTG: Isopropyl β-D-1-Thiogalctopyranoside, MW: Molecular Weight, NDEL1: Nuclear Distribution Element-Like 1, NPAS3: Nuclear PAS domain protein 3, PH: Pleckstrin Homology, SEC: Size Exclusion Chromatography, Tara: Trio-Associated Repeats on Actin, TRIOBP: Trio-Binding Protein.

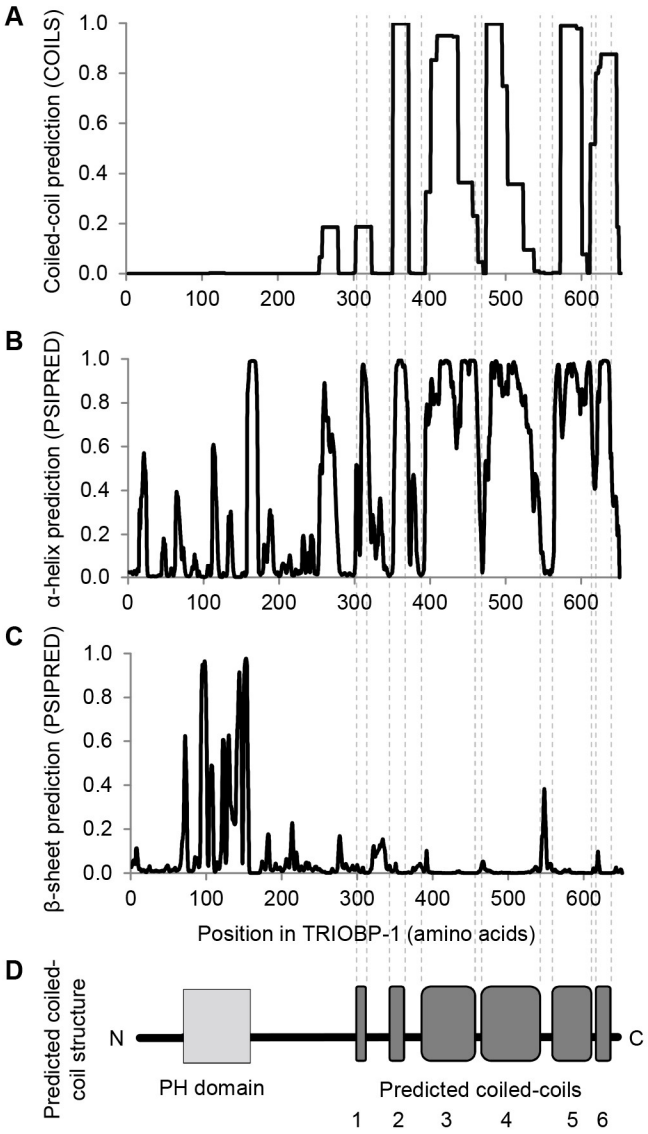

FIGURE 1: **Predicting the coil structure of TRIOBP-1**. (A) Prediction of coiled-coil forming propensity of the 652 amino acid TRIOBP-1 reading frame using the COILS server with a 21-amino acid sliding window. (B) Prediction of α-helix forming propensity using the PSIPRED server. (C) Prediction of β-sheet forming propensity using the PSIPRED server. (D) Proposed coiled-coil regions of TRIOBP-1 based on this data, shown in line with the graphs. The predicted Pleckstrin Homology, PH, domain is also displayed.

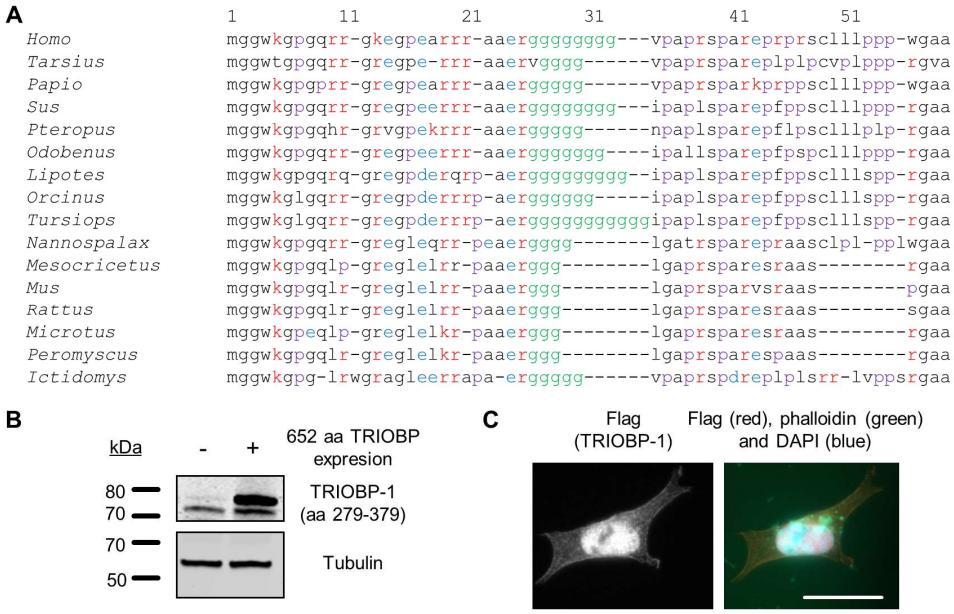

FIGURE 2; **The extreme N-terminus of TRIOBP-1**. (A) The putative initial 59 amino acids, aa, of TRIOBP-1, as present in multiple mammalian lineages. Notably, despite variation in amino acid sequence, and particularly in a poly-glycine stretch (green), all maintain the same reading frame. Positively charged residues are shown in red, negatively charged residues in blue and prolines in purple. Aligned using Clustal Omega (48) (http://www.ebi.ac.uk/Tools/msa/clustalo) and then manually curated. RefSeq accession number for the sequences shown are, in order displayed: NP_008963.3; XP_008065523.1; XP_009215517.1, XP_003126108.2; XP_006914811.1; XP_004410876.1; XP_007454108.1; XP_004279508.1; XP_004312195.1; XP_008849513.1; XP_005067025.1; XP_005067025.1; NP_001019887.1; XP_006242072.1; XP_005354277.1; XP_006979187.1; XP_005322324.1. (B) SH-SY5Y cells inducibly expressing the 652 aa species of TRIOBP-1, with and without induction of expression. The endogenous TRIOBP-1 species is seen to be of a slightly lower molecular weight than the 652 aa over-expressed protein, although a small amount of endogenous protein of this size is present, consistent with only a small portion of endogenous TRIOBP-1 protein expressing or maintaining the extreme N-terminus. (C) Expression of the N-terminal 59 aa of TRIOBP-1 alone in SH-SY5Y cells with a Flag tag.

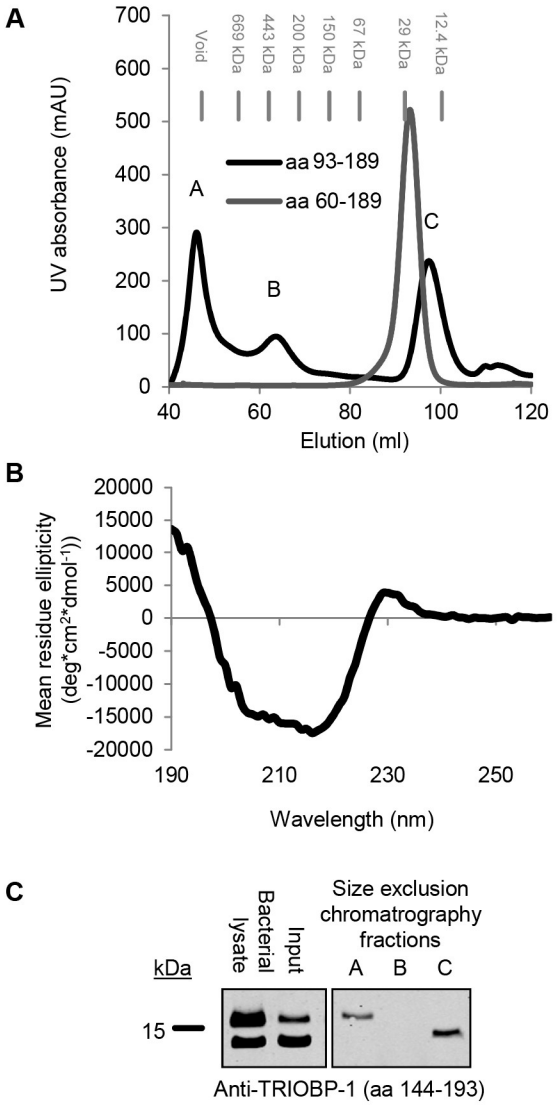

FIGURE 3: **Completeness of the Pleckstrin Homology (PH) domain is required for a stable recombinant protein fragment.** (A) SEC of recombinant proteins equating to the complete (aa 60-189) or incomplete (aa 93-189) PH domain of TRIOBP-1. The complete domain exists as a single clear species, while the incomplete one exists as multiple species, labeled A-C, including one in the void volume. (B) CD measurement of the aa 60-189 TRIOBP-1 fragment shows it to be folded and principally helical. (C) Western blot of aa 93-189 species from part A, reveals only a breakdown product to exist in the soluble fractions, as opposed to the void volume.

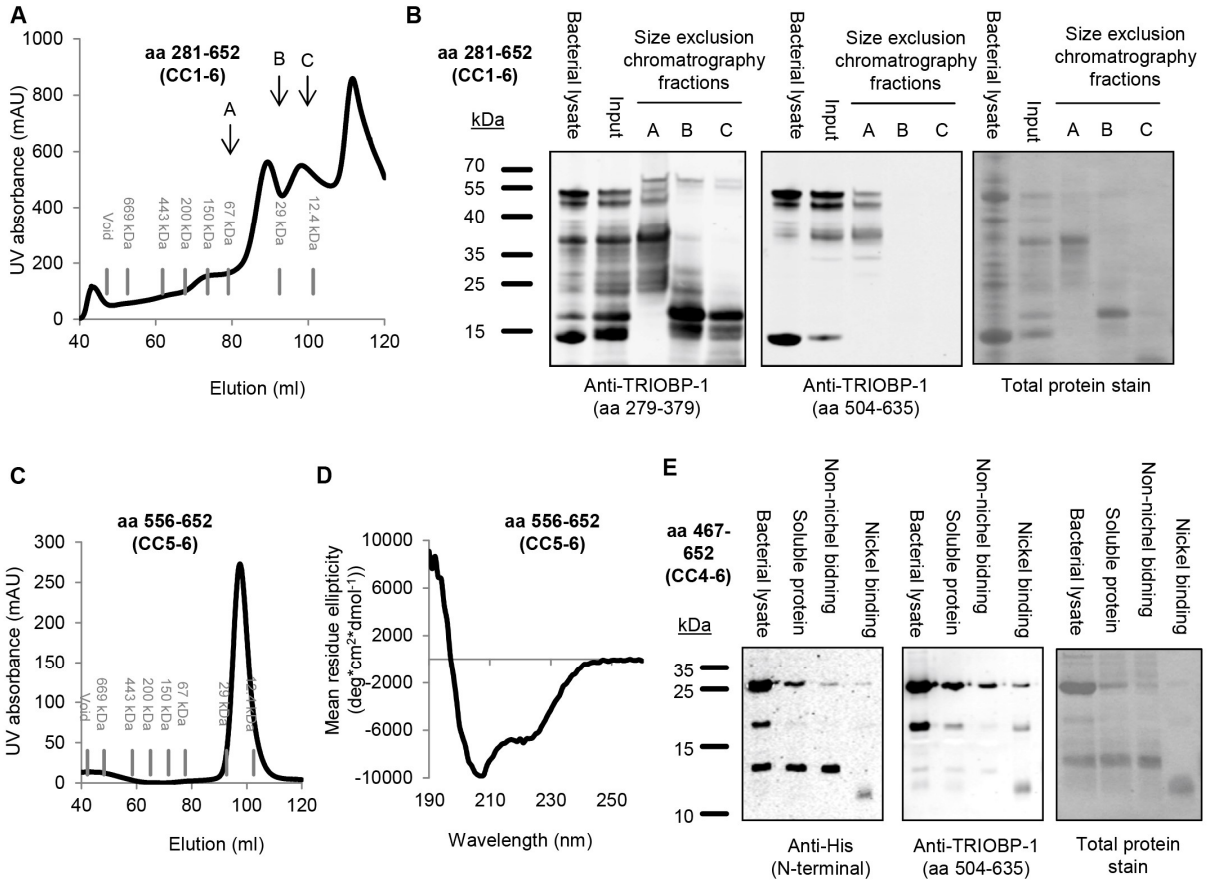

FIGURE 4: **TRIOBP-1 contains two distinct coiled-coil domains, as determined by expression of recombinant protein fragments**. (A) SEC of recombinant TRIOBP-1 coiled coils, CC, 1-6, aa 281-652. (B) SDS-PAGE and western blot of the whole lysate from bacteria expressing this fragment, nickel affinity purified protein ("input") and the chromatography fractions indicated in part A, after being concentrated. The protein breaks down into distinct fragments. (C) SEC of CC5-6, aa 556-652, revealing a single stable protein species. (D) Circular dichroism profile of the major CC5-6 species. (E) Recombinant TRIOBP-1 CC4-6, aa 467-652) breaks down prior to nickel affinity purification.

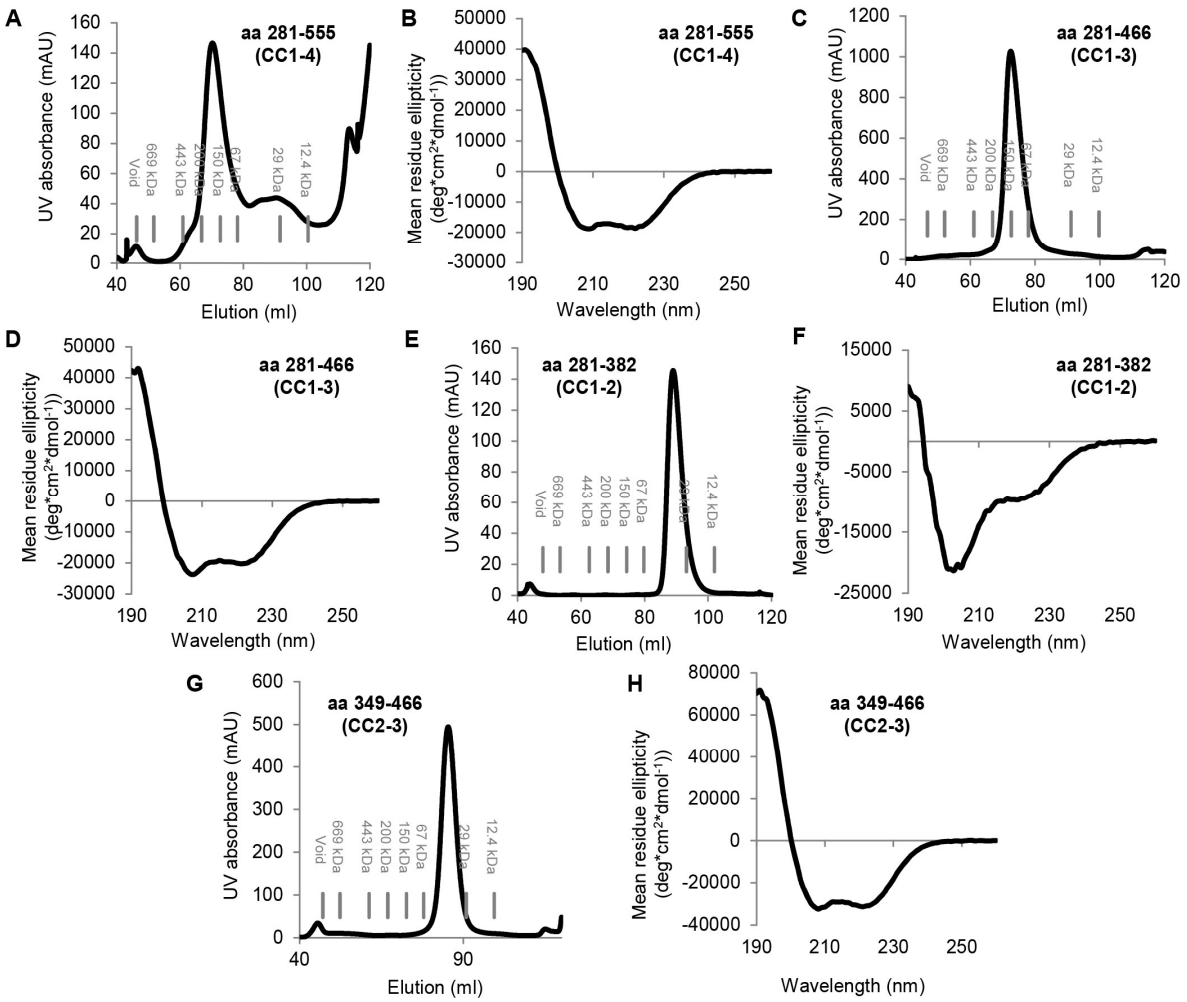

FIGURE 5: **The central domain of TRIOBP-1 is responsible for its oligomerization.** SEC and CD measurements of different combinations of the coiled-coils which make up the central domain of TRIOBP-1. (A) SEC of aa 281-555. (B) CD of the principle oligomeric state of aa 281-555. (C) SEC of aa 281-466. (D) CD of aa 281-466. (E) SEC of aa 281-382. (F) CD of aa 281-382. (G) SEC of aa 349-466. (H) CD of aa 349-466.

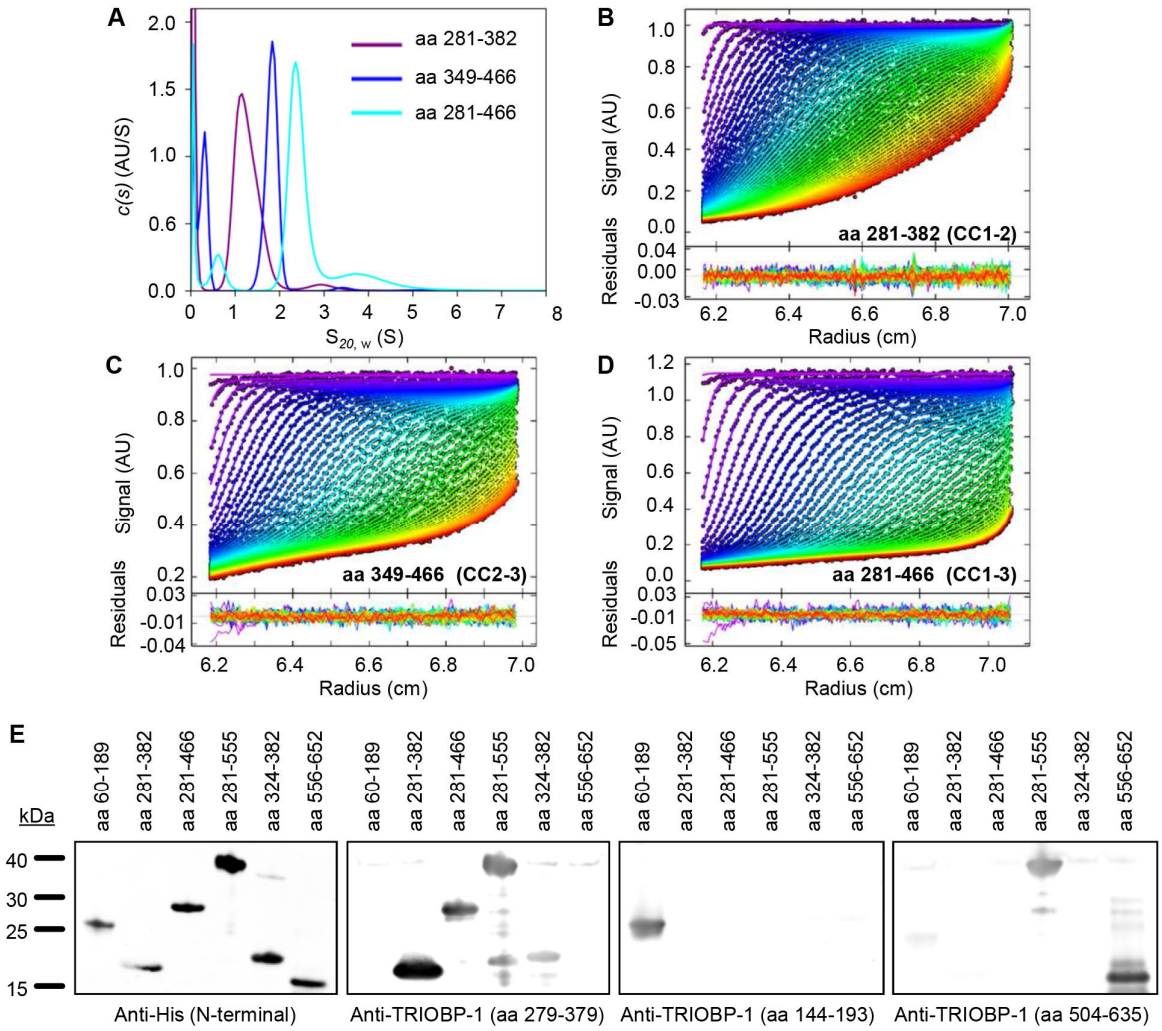

FIGURE 6: **The oligomeric state of the central domain, analyzed by analytical ultracentrifugation**. (A) SEC sedimentation velocity data performed on three fragments of the TRIOBP-1 central domain, with c(*s*) fit results shown. (B) Sedimentation profiles (dots) over time for the aa 281-382 fragment, 65 µM, experiment in part A, from purple (initial scan) to red (final, scans taken at 3 minute intervals), together with the *c*(*s*) fit results (lines). Below the graphs, the corresponding residuals are shown. (C) Equivalent sedimentation profile for the aa 349-466 fragment, 55 µM. (D) Equivalent sedimentation profile for the aa 281-466 fragment, 50 µM. (E) Western blot of the soluble TRIOBP-1 fragments used for these assays, with polyclonal antibodies raised against different parts of the protein used to distinguish them. Note that some degradation of the aa 281-555 construct can be seem, yielding a fragment corresponding approximately to the aa 281-382 or 324-382 constructs. This is not seen for the aa 281-466 construct. The left two panels were stained from one membrane, and the right two panels from another displaying identical samples.

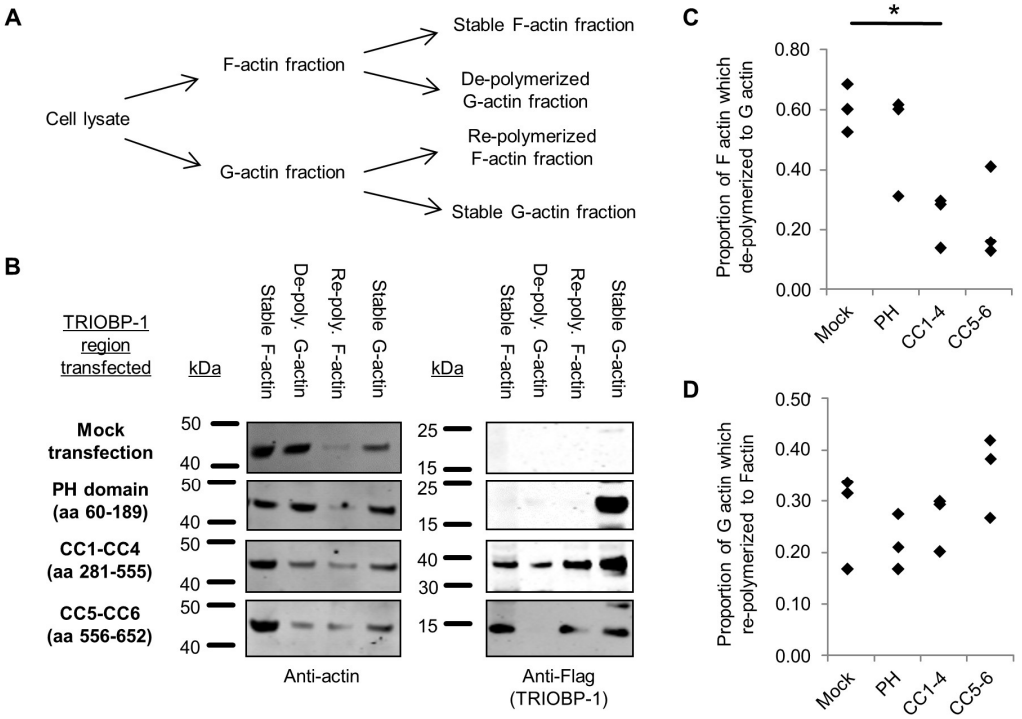

FIGURE 7: **The effect of TRIOBP-1 subdomains on actin dynamics**. (A) Scheme of the actin assay performed. Cell lysate from NLF neuroblastoma cells was separated by ultracentrifugation into F-actin and G-actin-containing fractions. The stability of the separated F-actin was assayed by incubating it in a depolymerization buffer, and then separating again by ultra-centrifugation into a (stable) F-actin-containing fraction and a (de-polymerized) G-actin fraction. Similarly, the stability of G-actin was assayed by incubating it in polymerization buffer and then separating it into a (stable) G-actin-containing fraction and a (re-polymerized) G-actin fraction. (B) Western blots of the ensuing fractions, showing the abundance of actin and of Flag-tagged TRIOBP-1 fragments which had been transfected in. All actin blots are shown under equivalent conditions, as are the top three Flag-blots. The lowest Flag blot is shown under a higher gain, due to the much lower level of the aa 556-652 protein after transfection (approximately 5-fold lower than aa 281-555). (C) Quantification of the proportion of actin in the original F-actin fraction which transferred to the G-actin fraction after incubation under de-polymerization conditions. (D) Quantification of the proportion of actin in the original G-actin fraction which transferred to the F-actin fraction after incubation under polymerization conditions. In both graphs n = 3, *: $p < 0.05$, according to a paired t-test after correction for multiple testing.

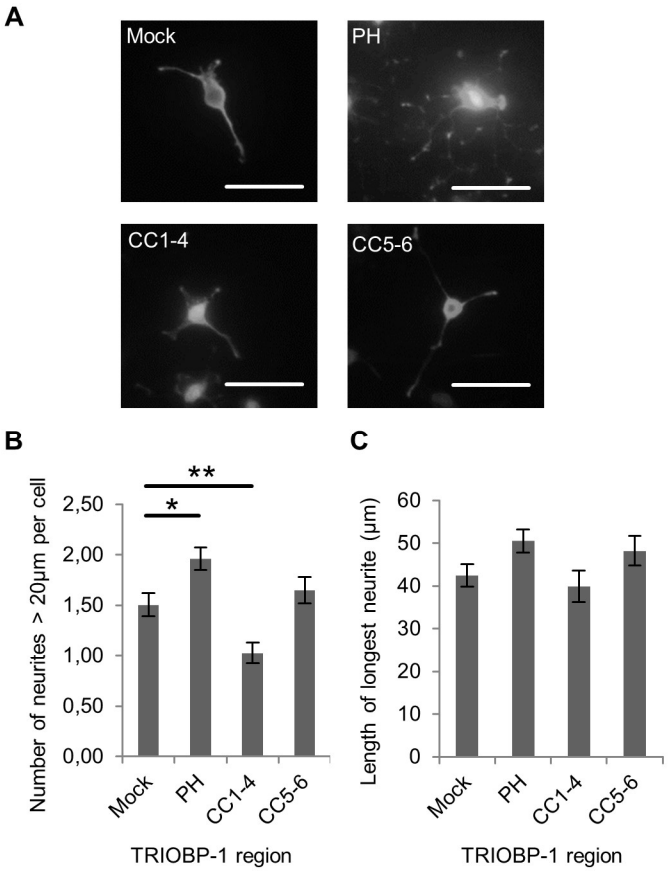

FIGURE 8: **The effect of TRIOBP-1 subdomains on neurite outgrowth**. (A) Sample images of Neurosreen-1 cells transfected with either an empty vector ("Mock", n = 171) or one of the following TRIOBP-1 fragments: aa 60-189 ("PH", n = 174), aa 281-555 ("CC1-4", n = 161) and aa 556-652 ("CC5-6", n = 152). Color has been deliberately over-exposed to ensure all neurites are visible. Scale bars represent 50 µm. (B) The mean number of neurites per cell (defined as any outgrowth over 20 µm in length) shows the PH domain alone to increase neurite number, and the central domain to decrease it. *: $p < 0.05$, **: $p < 0.01$ after correction for multiple testing. (C) Mean length of the longest neurite in each cell. The PH domain has a trend effect, significant before but not after correction for multiple testing. All values were compared by one-way ANOVA with Bonferroni correction to the "Mock" value.

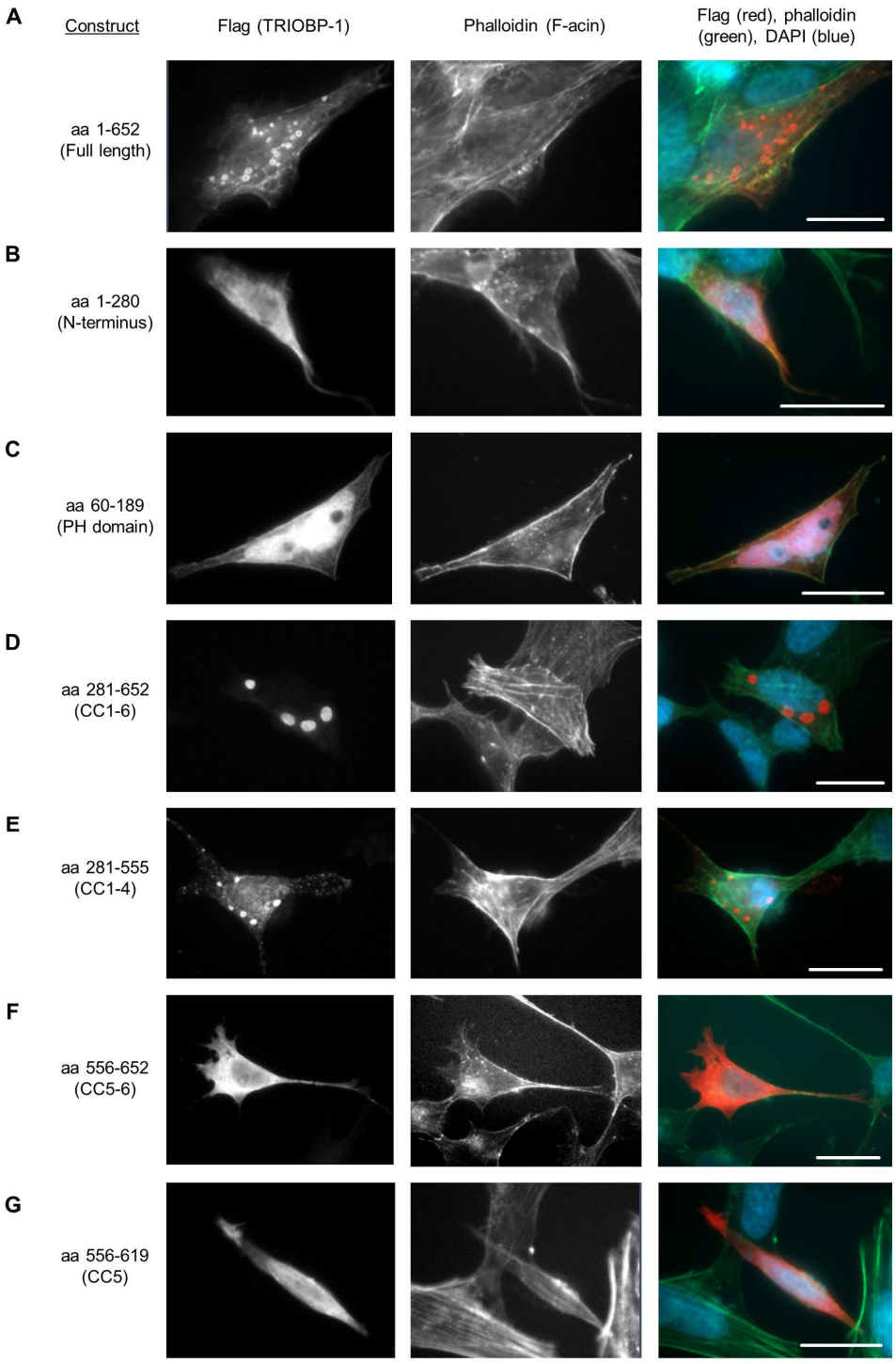

FIGURE 9: **Subcellular localization and aggregation propensity of TRIOBP-1 fragments in neuroblastoma cells**. Flag-tagged TRIOBP-1 protein fragments were transfected into SH-SY5Y cells and then visualized using an anti-Flag antibody and immunoflorescence microscopy. F-actin was visualized using florescent-labeled phalloidin. For each construct, the amino acid, aa, position in full length TRIOBP-1 is displayed. All scale bars represent 20 µm. (A) The full length protein, aa 1-652, which aggregates. (B) The N-terminal region, aa 1-280. (C) The PH domain, aa 60-189. (D) CC1-6, aa 281-652, which forms aggregates. (E) CC1-4, aa 281-555, which forms aggregates. (F) CC5-6, aa 556-652. (G) CC5, aa 556-619.

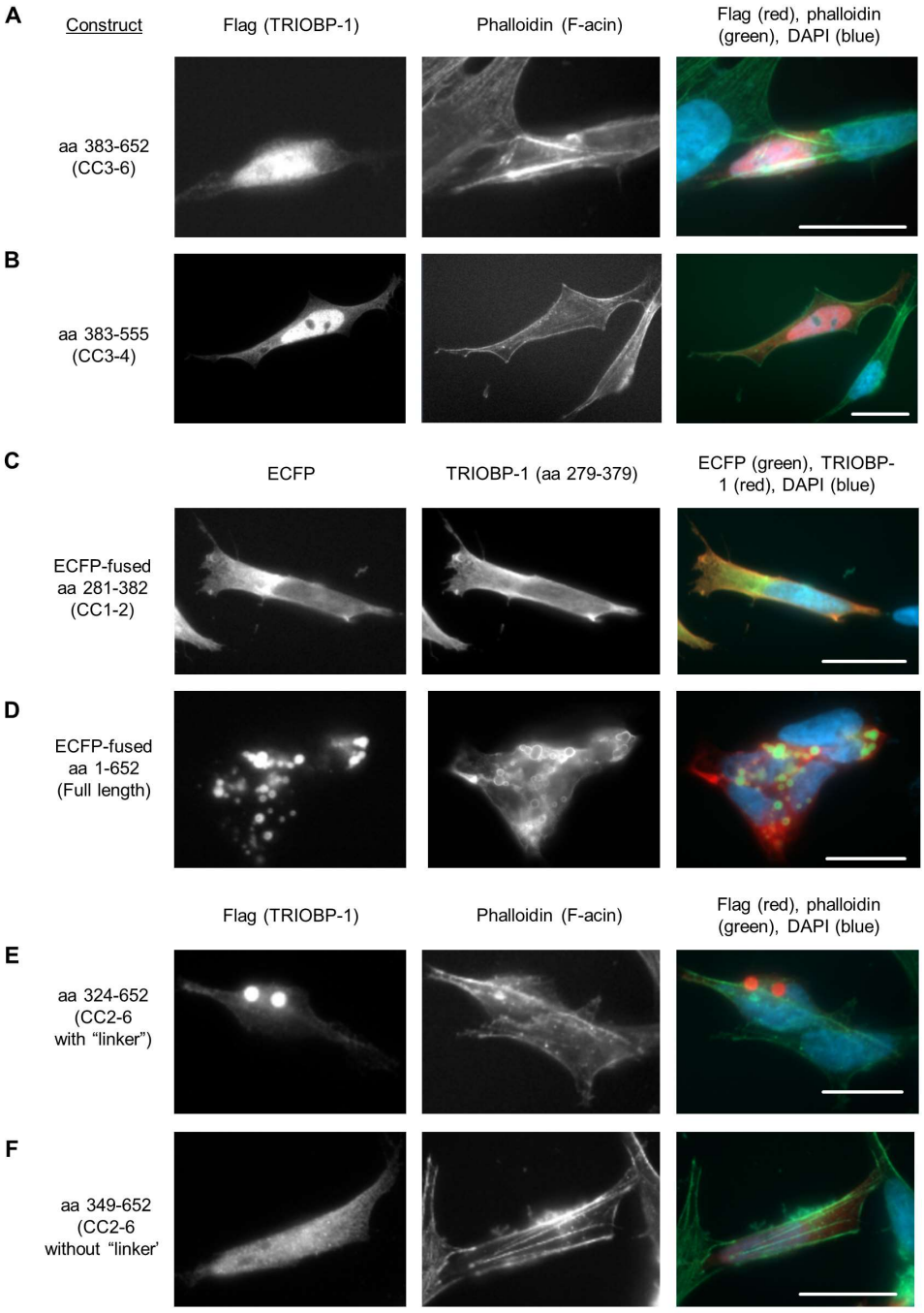

FIGURE 10: **Further subcellular localization and aggregation propensity of TRIOBP-1 fragments in neuroblastoma cells**. Flag-tagged TRIOBP-1 protein fragments were transfected into SH-SY5Y cells and then visualized using an anti-Flag antibody and immunofluorescence microscopy. F-actin was visualized using florescent-labeled phalloidin. For each construct, the amino acid, aa, position in full length TRIOBP-1 is displayed. All scale bars represent 20 µm. (A) CC3-6 of TRIOBP-1, encoded by aa 383-652. (B) CC3-4, aa 383-555. (C) CC1-2, aa 281-382, however for this image an ECFP-fused construct was used and so anti-TRIOBP-1 antibody is used alongside the ECFP florescence to visualize the protein. (D) The full length protein, aa 1-652, with a ECFP fusion protein. Note, that while ECFP stains the whole aggregate, an anti-TRIOBP-1 antibody stains only the periphery. This is consistent with previous reports of TRIOBP-1 aggregates (28) and likely represents the antibody being unable to penetrate the core of the densely packed protein aggregate. (E) CC2-4, including the 25 aa linker between CC1 & CC2, aa 324-652, which forms aggregates. (F) CC2-4, excluding the 25 aa linker between CC1 & CC2, aa 349-652.

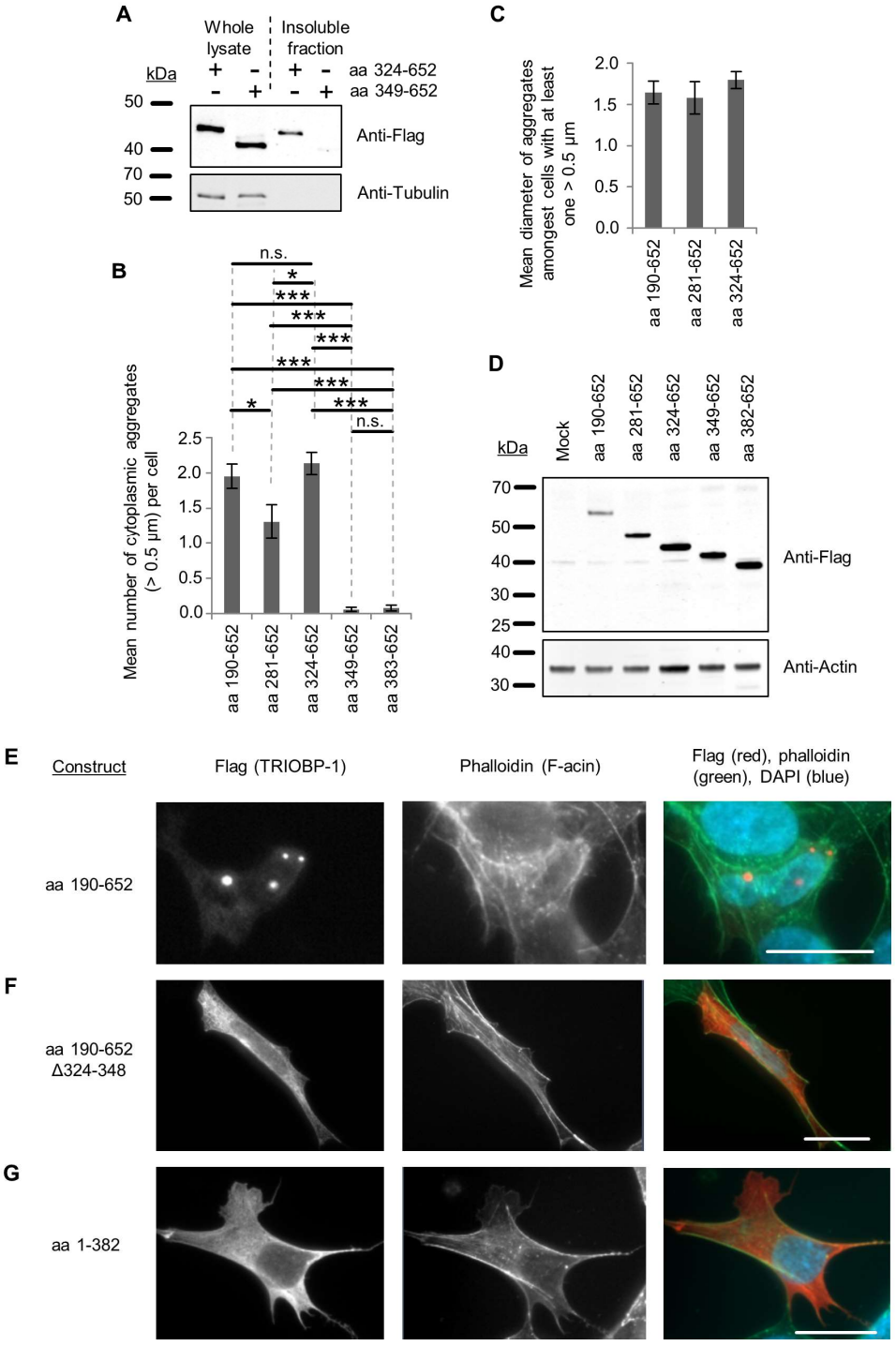

FIGURE 11: **Confirmation of an aggregation-critical region between coiled-coils 1 and 2 of TRIOBP-1**. (A) Cell lysates and corresponding purified insoluble protein pellets of SH-SY5Y cells expressing Flag-tagged TRIOBP-1 aa 324-652 or 349-652. (B) In a blinded experiment, cells were transfected with TRIOBP-1 fragments and the mean number of aggregates per cell was quantified. Standard errors of the mean are shown, along with p-values determined by one-way ANOVA, with Bonferroni correction for multiple testing. Constructs used encoded TRIOBP-1 aa 190-652 (n = 65), aa 281-652 (n = 71), aa 324-652 (n = 72), aa 349-652 (n = 71) or aa 383-652 (n = 65). Over the whole dataset, $p < 0.001$. ns: not significant; *: $p < 0.05$, ***: $p < 0.001$. (C) In the same experiment, the mean diameter of Flag-positive aggregates did not vary significantly between constructs. (D) Western blot of lysates from SH-SY5Y cells transfected with the TRIOBP-1 constructs used in the blinded aggregation assay. (E) Flag-tagged TRIOBP-1 protein fragment aa 190-652 transfected into SH-SY5Y

cells. (F) Transfection of an identical construct lacking the aggregation critical region aa 324-348. (G) Transfection of a construct encoding TRIOBP-1 aa 1-382. All scale bars represent 20 μm.

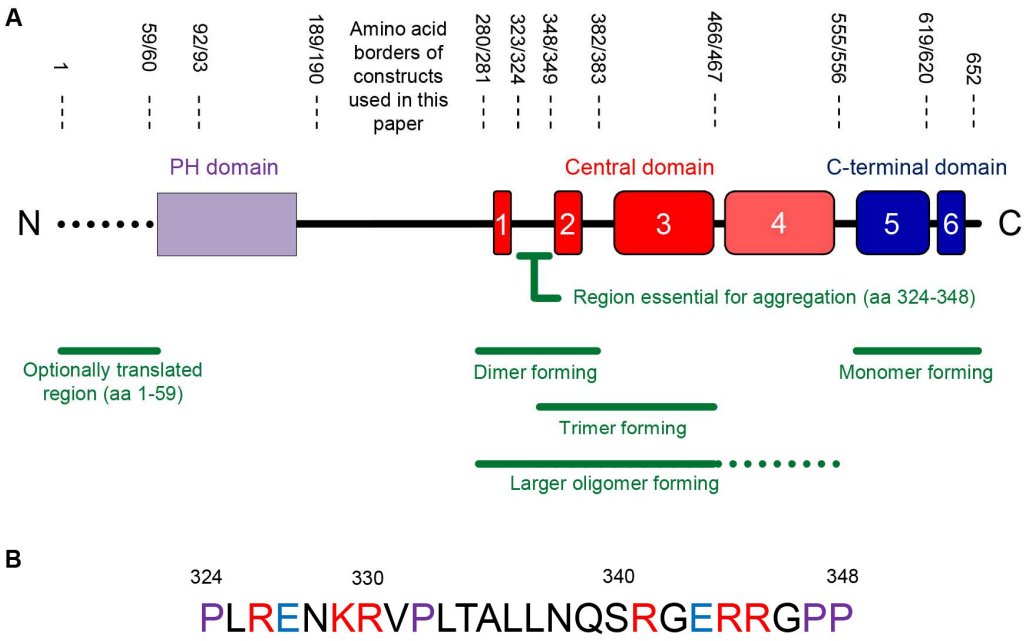

FIGURE 12: **Summary of the domain structure of TRIOBP-1**. (A) The Pleckstrin Homology (PH, purple) domain and coiled coil regions of TRIOBP-1 are shown. Coiled coils are divided between those which constitute the central domain (CC1-CC3 and possibly CC4, red) and the C-terminal domain (CC5-CC6). Regions of interest are indicated in green, including the aggregation critical region and the oligomeric states of selected fragments of TRIOBP-1 when expressed as recombinant proteins. (B) Sequence of the 25 amino acid region found to be essential for aggregation. It is rich in prolines (shown in purple) and charged residues (red for positive charge, blue for negative).

	PH domain	Central domain	C-terminal domain
Location on TRIOBP-1			
Amino acids	60-189	281-555	556-652
Coiled-coils	N/A	1-4	5-6
Actin assay			
Segregates with F-actin	No	Yes	Yes
Segregates with G-actin	Yes	Yes	Yes
Effect on F-actin de-polymerization	No effect	Inhibition	Trend inhibition
Effect on G-actin polymerization	No effect	No effect	Trend promotion
Neurite assay			
Effect on neurite number	Increase	Decrease	No effect
Effect on longest neurite length	Trend increase	No effect	No effect

TABLE 1: **Summary of functional assays performed on isolated domains of TRIOBP-1.** Based on data found in figures 7 and 8.